京都大学防災研究所年報 第 55 号 B 平成 24 年 6 月
Annuals of Disas. Prev. Res. Inst., Kyoto Univ., No. 55 B, 2012

Numerical and Experimental Study on Debris-flow breaker

Yeonjoong Kim(1), Hajime NAKAGAWA, Kenji KAWAIKE and Hao ZHANG

(1) Graduate School of Engineering, Kyoto University

Synopsis

Main function of debris-flow breaker is effectively stopping a debris flow front. Debris-flow breakers have advantage not only to reduce the energy but also to create suitable narrow area, cost-efficient, simply designed, easily repaired and maintained. However, the mechanism of the debris-flow breaker has not been explained. In this paper, fundamental experiments and numerical simulation are conducted to investigate debris-flow breakers. In addition, a methodology is proposed to assess the suitability of a variable deck size and change of pressure on the deck according to separation of water. As a result, it has been acquired as relationship between optimum sizes and width of deck, maximum diameter and geometric standard deviation for sediment A, B and C. Furthermore, the simulated results of the travel length and deposit thickness on the deck are also compared with experimental results.

Keywords: debris flow, pore water pressure, optimum size, debris-flow breaker

1. Introduction

Debris flows are common in mountainous areas throughout the world, which contain varying amounts of mud, sand, gravel, boulders, and water. In addition to causing significant morphological changes along riverbeds and mountain slopes, these flows are frequently reported to have brought about extensive property damage and loss of life (Takahashi, 1991; Hunt, 1994; Huang and Garcia, 1997). Therefore, the understanding of behavior and mechanism of debris flow and the study of preventive measures are very important in order to manage the sediment disaster in the river basin and prevent the downstream hazards. To reduce the debris flow hazards, it is common to couple structural and non structural preventive measures. Preventive measures require the consideration of the various scenarios and involve the evaluation of hydrological, hydraulic, sediment size distribution, topographical and other parameters.

Table 1 shows the occurrence of sediment related disaster in 2009 Japan (MLIT, 2009). However, occurrence of debris flow disaster is relatively very small about 14% recorded. But if debris flow occurs, bring about huge damage. Especially, it has recorded 17 (77%) human death tolls. So we have to improve structural and non-structural measures for preventive disaster.

Usually, sediment control structures temporarily stores the excess sediment in the upstream pocket of sabo dam and reduce discharge safely. The capacity of sabo dam to control sediment is determined by sediment storage capacity between the stable slope and the temporary slope of accumulated sediments. Therefore, sabo dam should control the increasing amount of sediment discharge due to gradually accelerating of debris flow. Using the debris-flow breaker at upstream of a sabo dam, could be more effective to control sediment discharge than without debris-flow breaker. The peak discharge of the flow must have been effectively reduced and the flow converted to a less-harmful level because of the

Table 1 Occurrence of sediment related disaster in 2009 (Japan)

Cause	Incidence	Human suffering			Structure		
		Dead	Missing	Injured	Complete destruction	Partial destruction	Some Damage
Debris flow	(14%) 149	(77%) 17	0	2	13	10	65
landslide	(10%) 106	0	0	0	5	1	10
Slope failure	(76%) 803	(23%) 5	0	11	6	15	140
Total	1,058	22	0	13	24	26	215

reduced size of the boulder dam and the frontal part of the debris flow was trapped as shown in Photo 1 (Suwa et al, 2009).

Main of function debris-flow breaker is effectively stopping a debris flow front. It has advantage not only to reduce the energy but also to create suitable narrow area (Photo 2), cost-efficient, simply designed, easily repaired and maintained if their size and location are well planned before construction (ICHARM, 2008).

It is thought that two phenomena occur when a debris flow crosses the debris-flow breaker: the pore (mud) water drains through the deck of the debris-flow breaker and the pore water pressure near the deck changes (Gonda, 2009). Drainage of the pore water through the deck increases the sediment concentration of the debris flow increasing the bottom shear stress of the debris flow. Because the deck of the debris-flow breaker is open to the air, the pore water pressure of the debris flow near the deck decreases instantaneously.

Watanabe, et al.(1980) has shown that the spacing of the posts has effects on the trapping capacity of a slit dam. When the relative spacing $l_o / d_{\max} < 2.0$, where l_o is the spacing of the posts and $d_{\max}$ is the maximum diameter of the debris flow, the volume of the debris flow could be reduced by 50% during peak time. The above studies validated the effectiveness of open-type dams in the prevention of debris flow. They all only considered the relative spacing factor in designing the spacing of open-type dams.

In this paper, to improve hard countermeasures according to fundamental experiments and numerical simulation are conducted to investigate debris-flow breakers. A methodology proposed to assess the suitability of a variable deck size and change of pressure on the deck according to separation of water. To consider change of pore water pressure, modify to

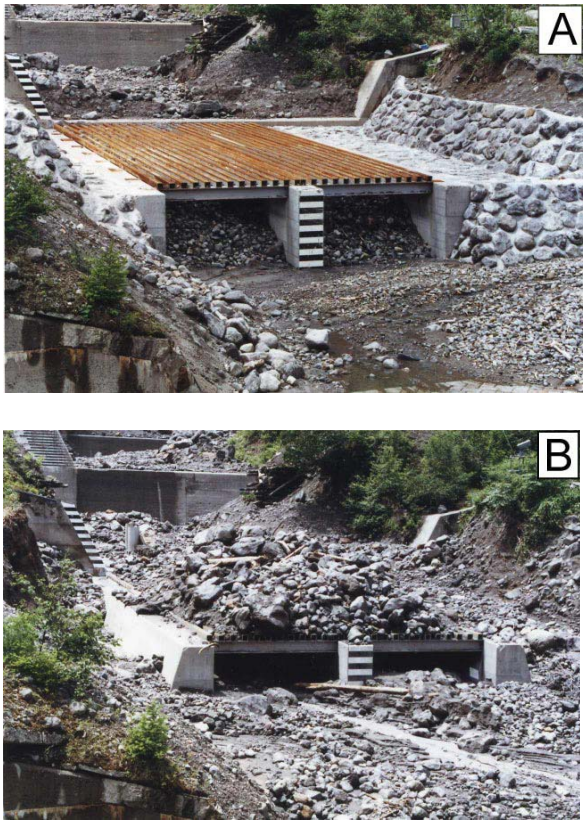

Photo 1 Flat-board debris-flow breaker. (A) After removal of the July 21, 1985 debris-flow deposits and the construction of sidewall reinforcements. (B) Boulder deposits of the July21, 1985 debris flow trapped on the breaker (photo taken July 22, 1985).

Photo 2 Suitable narrow area.

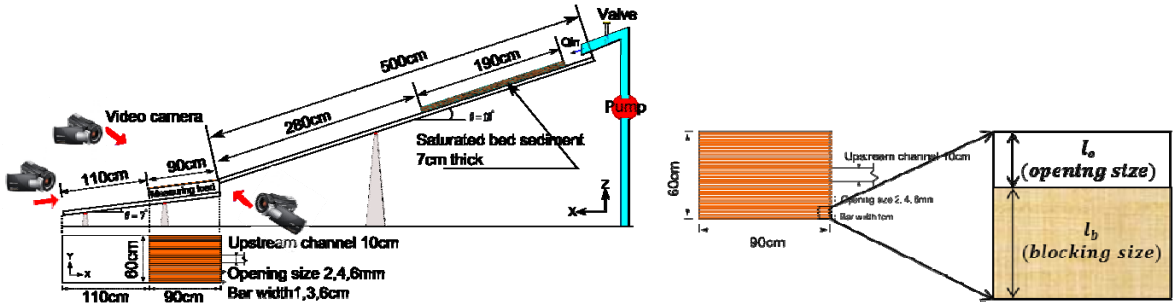

Fig.1 Experimental flume setup

momentum equation of pressure term using kinetic boundary conditions due to γ coefficient at debris-flow breaker. As a result, it is able to verify the impact of different deck conditions according to variation of opening and blocking size. In addition, it is possible to decide the optimum size by relationship between opening size, width, max diameter and geometric standard deviations. Furthermore, the simulated results of the travel length and deposit thickness on the deck are also compared with experimental results.

2. Laboratory experiments

A rectangular flume of 5m long, 10cm wide and 13cm deep is used for the experiments. The slopes of flume are set at upstream with 18°and downstream with 7°. The details of experiment setup are shown in

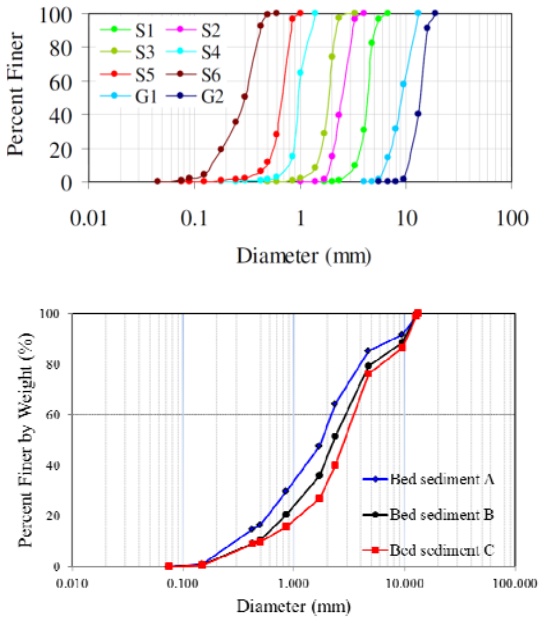

Fig.2 Grain size distribution curve of sediment materials

Table 2 Properties of sediment material

Sediment	$D_{mean}(mm)$	$D_{95}(mm)$	σ_g	k_d
A	1.783	10.871	3.083	0.341
B	2.304	11.142	3.217	0.353
C	3.054	11.163	3.140	0.363

Table 3 Experimental conditions

Case No.	Upstream	Blocking size	Opening size
Case-0-0.0-A,B,C	S-A S-B S-C	0.0	0.0
Case-1-0.2-A,B,C		1.0	0.2
Case-1-0.4-A,B,C			0.4
Case-1-0.6-A,B,C			0.6
Case-3-0.2-A,B,C		3.0	0.2
Case-3-0.4-A,B,C			0.4
Case-3-0.6-A,B,C			0.6
Case-6-0.2-A,B,C		6.0	0.2
Case-6-0.4-A,B,C			0.4
Case-6-0.6-A,B,C			0.6

Unit : cm

Fig. 1. Silica sand (S1, S2, S3, S4, S5, S6) and gravel (G1) are mixed in equal proportion by weight to prepare the bed sediment-A. Silica sand (S1, S2, S3, S4, S5, S6) in proportion (1.6, 1.5, 1, 1, 1, 0.7) and gravel (G1) in (1.7) by weight are mixed to prepare the bed sediment-B. Silica sand (S1, S2, S3, S4, S5, S6) in proportion (2.6, 1.7, 0.7, 0.7, 0.7, 0.6) and gravel (G1) in (2.0) by weight are mixed to prepare the bed sediment-C. Fig.2 shows particle size distribution of the prepared material for bed sediment-A, bed sediment-B and bed sediment-C. The bed sediment with 1.9m long and 7cm deep is positioned 2.8m upstream from the outlet of the flume by installing a partition of 7cm in height to retain the sediment. This sediment bed is saturated

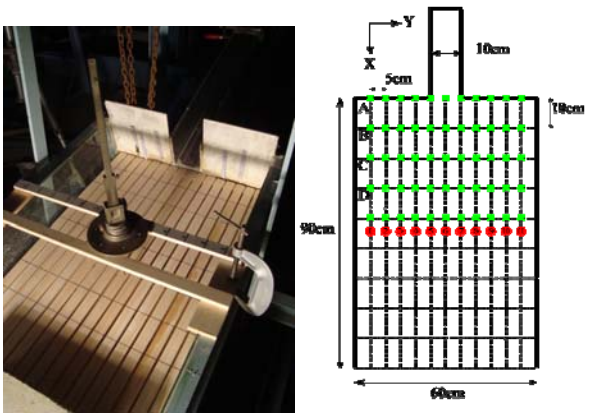

Fig.3 Observation points on the debris-flow breaker

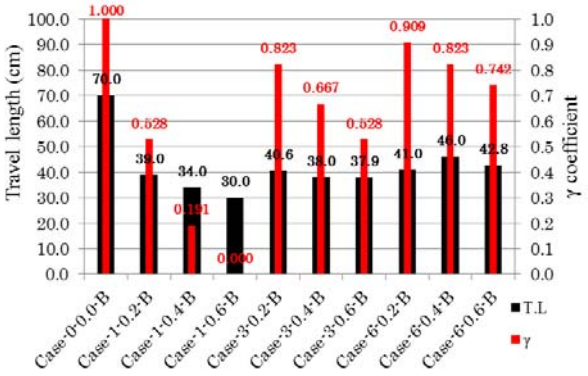

Fig.5 Compare to travel length and γ coefficient

by water. Properties of sediment material and experimental condition are shown in Table 2 and Table 3. Maximum sediment concentration at bed $C_* = 0.65$, angle of repose $\tan\phi = 0.7$ and sediment density $\sigma = 2.65g/cm^3$ are used. Debris flow is produced by supplying a constant water discharge of $300cm^3/\sec$ for $10\sec$ from upstream end of the flume. Debris flow produced in the experiments is the fully stony type debris flow and the largest particles are accumulated in the forefront. To measure the thickness of deposition (i.e. the flow depth plus the deposition thickness in the final stage) accurately, a vernier point gauge is used in each point (Fig. 3).

3. Numerical model

3.1 Change of pore water pressure

The debris-flow breaker is a simple engineering structure which filters fine sediment with water and traps the course debris on a horizontal screen. It was designed to separate coarse clastic debris from water with a fine debris matrix so that the water passes through the breaker board while the coarse debris flow is trapped. When the debris flow reaches the deck, the infiltration occurs rapidly which can changes the pore water pressure (Fig. 4). But until now, the mechanism of the debris-flow breaker structure has not been well explained. Previous study

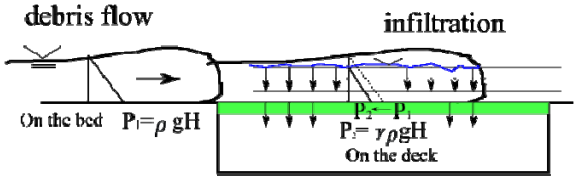

Fig.4 Pore water pressure distribution on the debris flow

(Gonda, 2009) suggested that change in pore water pressure is due to the γ factor using 1D dynamic model.

Previous study considered only permeability of deck and porosity of sediment. But we found the need for modify previous γ coefficient. Because of previous γ coefficient is no coherence with all cases. Specially, experimental results of travel length (case1-0.2-B, case3-0.2-B and case6-0.2-B) are recorded around 40.0cm. Result of travel length very similar, but γ coefficients have very different value in each case. Fig. 5 shows that the result of travel length and γ coefficient depends on blocking size and opening size with sediment B. So that determined new γ coefficients are estimated by empirical equations.

$$\gamma = \begin{cases} 1 & : \ on \ \ the \ \ bed \\ 1 - \left[\dfrac{k_s}{k_d} \times Impact \ \ of \ \ loss \right]^{\beta} & : \ on \ \ the \ \ deck \end{cases} \quad (1)$$

$$Impact \ \ of \ \ loss = 1 - \left(\frac{N_h}{W}\right)$$

$$N_h = \left[\frac{2\left(\sum l_o \times \sum l_b\right)}{\sum l_o + \sum l_b} \right] \quad (2)$$

where k_s is permeability of deck, k_d is sediment of porosity, l_o and l_b are opening size and blocking size, W is the width in the deck and β is the constant coefficient (0.3).

New γ coefficient (1) included an impact of loss factor (2). Impact of loss factors indicate that effective between opening size and blocking size by

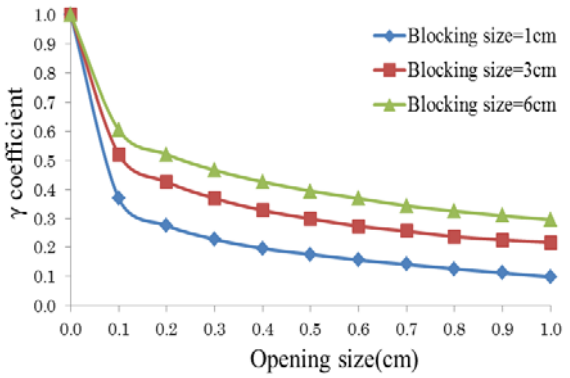

Fig. 6 Variation of γ coefficient (sediment B)

t-test method (Ralph L. R, et al. 2000). This analysis is appropriate whenever you want to compare the impact of two groups. Fig. 6 shows that relation γ coefficient depend on variation of blocking size and opening size using Eq. (1).

3.2 Governing equation

The basic equations used to compute the behavior of flow motion of debris flow are the two-dimensional momentum equations, continuity equation of flow, continuity equation of sediment and river bed surface equation. The pore water pressure will be changed on the debris-flow breaker due to γ factor relationship. Momentum equations of pressure term could be integrated assuming the kinetic boundary conditions at bed $(=\rho gh)$ and water surface $(=0)$. But, bed kinetic boundary condition is not ρgh on the deck. To consider change of the pore water pressure the bed kinetic boundary condition could be changed from ρgh to $\gamma\rho gh$ at the deck. By introducing these pore water pressure at the debris-flow breaker, the depth-wise averaged two-dimensional momentum equations of debris flow for the x–wise (down valley) and y-wise (lateral) directions are described as follows.

$$\frac{\partial M}{\partial t}+\beta\frac{\partial(uM)}{\partial x}+\beta\frac{\partial(vM)}{\partial y}=gh\sin\theta_{bx0}-gh\cos\theta_{bx0}\frac{\partial(z_b+h)}{\partial x}$$
$$-(gh-\gamma gh)(\sin\theta_{bx0}-\cos\theta_{bx0}\frac{\partial z_b}{\partial x})-\frac{\tau_{bx}}{\rho_T} \quad (3)$$

$$\frac{\partial N}{\partial t}+\beta\frac{\partial(uN)}{\partial x}+\beta\frac{\partial(vN)}{\partial y}=gh\sin\theta_{by0}-gh\cos\theta_{by0}\frac{\partial(z_b+h)}{\partial y}$$
$$-(gh-\gamma gh)(\sin\theta_{by0}-\cos\theta_{by0}\frac{\partial z_b}{\partial y})-\frac{\tau_{by}}{\rho_T} \quad (4)$$

The continuity equation of the total volume is

$$\frac{\partial h}{\partial t}+\frac{\partial M}{\partial x}+\frac{\partial N}{\partial y}=i_b \quad (5)$$

The continuity equation of the coarse particle fraction that is sustained in the flow by the action of particle encounters is

$$\frac{\partial(C_L h)}{\partial t}+\frac{\partial(C_L M)}{\partial x}+\frac{\partial(C_L N)}{\partial y}=\begin{cases} i_b C_{*L} & (i_b\geq 0)\\ i_b C_{*DL} & (i_b<0)\end{cases} \quad (6)$$

where $M\ (=uh)$ and $N\ (=vh)$ are flow flux in x, y directions, u and v are the mean velocity, h is flow depth, i_b is erosion (>0) or deposition (≤ 0) velocity, C is the sediment concentration in the flow, C_* is maximum sediment concentration in the bed, β is momentum correction factor equal to 1.25 for stony debris flow (Takahashi et al., 1992), g is the acceleration due to gravity, θ is bed slope, τ_b is bottom shear stress, ρ_T is mixture density $(\rho_T=\sigma C+(1-C)\rho)$, σ is density of the sediment particle, and ρ is density of the water.

The equation for the erosion/deposition process to change in bed surface elevation is described as follows:

$$\frac{\partial z_b}{\partial t}+i_b=0 \quad (7)$$

where z_b is erosion or deposition thickness of the bed measured from the original bed surface elevation.

3.3 Bottom shear stress

In the upstream region of a debris-flow breaker, sediment concentration is higher than that of equilibrium state and becomes maximum concentration due to existence of the deck, and the yield stress exceeds the driving force, then debris flow stops and deposition occurs, before filling up upstream of the deck. This mechanism of deposition is incorporated in momentum equation of the flow mixture as considering yield stress in bottom shear stress. For a fully developed stony debris flow $(C_L>0.4C_*)$;

$$\tau_{bx}=\frac{u}{\sqrt{u^2+v^2}}\tau_{yx}+\rho f_b u\sqrt{u^2+v^2} \quad (8)$$

$$\tau_{by}=\frac{v}{\sqrt{u^2+v^2}}\tau_{yy}+\rho f_b v\sqrt{u^2+v^2} \quad (9)$$

in which τ_{yx} and τ_{yy} are the yield stresses in x and y directions, which can be expressed by using constitutive equations of Takahashi et al., (1997) as follows:

$$\tau_{yx} = f(C_L)(\sigma-\rho)C_L gh\cos\theta_x \tan\phi \tag{10}$$

$$\tau_{yy} = f(C_L)(\sigma-\rho)C_L gh\cos\theta_y \tan\phi \tag{11}$$

$$f(C_L) = \begin{cases} \dfrac{C_L - C_3}{C_* - C_3} & ;\ C_L > C_3 \\ 0 & ;\ C_L \le C_3 \end{cases} \tag{12}$$

where θ_x and θ_y are the x and y components of slope of the bed surface. C_s is the limitative sediment concentration(0.48). The coefficient of resistance, f_b, is described as

$$f_b = \frac{1}{8}\frac{(\sigma/\rho)}{\left(\left\{(C_*/C_L)^{1/3}-1\right\}^2\right)}\left(\frac{d_m}{h}\right)^2 \tag{13}$$

For an immature debris flow $(0.02 \le C_L \le 0.4C_*)$;

$$\tau_{bx} = \frac{\rho_T}{0.49}\left(\frac{d_m}{h}\right)^2 u\sqrt{u^2+v^2} \tag{14}$$

$$\tau_{by} = \frac{\rho_T}{0.49}\left(\frac{d_m}{h}\right)^2 v\sqrt{u^2+v^2} \tag{15}$$

For an immature debris flow $(C_L < 0.02)$;

$$\tau_{bx} = \frac{\rho g n^2 u\sqrt{u^2+v^2}}{h^{1/3}} \tag{16}$$

$$\tau_{by} = \frac{\rho g n^2 v\sqrt{u^2+v^2}}{h^{1/3}} \tag{17}$$

3.4 Erosion and deposition velocity equation

The erosion and deposition velocity that have been given by Takahashi et al., (1997) are used as follows.

Erosion velocity, if $C < C_\infty$;

$$i_b = \delta_e \frac{C_\infty - C_L}{C_* - C_\infty}\frac{\sqrt{u^2+v^2}\,h}{d_m} \tag{18}$$

Deposition velocity, if $C \ge C_\infty$;

$$i_b = \delta_d\left(1-\frac{\sqrt{u^2+v^2}}{pU_e}\right)\frac{C_\infty - C_L}{C_{*DL}}\sqrt{u^2+v^2} \tag{19}$$

where $P = (2/3)$ is numerical constant and U_e is the equilibrium velocity at which neither erosion nor deposition takes place as follows:

$$U_e = \frac{2}{5d_m}\left[\frac{g\sin\theta_e}{a_i\sin\alpha_i}\left\{C_L + (1-C_L)\frac{\rho_m}{\sigma}\right\}\right]^{1/2}\left\{\left(\frac{C_{*DL}}{C_L}\right)^{1/3}-1\right\}h^{3/2} \tag{20}$$

where θ_e channel slope in which coarse sediment concentration is in equilibrium, which can be obtained as follows.

$$\tan\theta_e = \frac{C_L(\sigma-\rho_m)\tan\phi}{C_L(\sigma-\rho_m)+\rho_m} \tag{21}$$

where ϕ is internal friction angle of sediment, δ_e (=0.0007) is erosion coefficient, δ_d (=0.01) is deposition coefficient, d_m is mean diameter of sediment and C_∞ is the equilibrium sediment concentration described as follows (Nakagawa et al., 2003), if $\tan\theta_w > 0.138$, a stony type debris flow occurs, and

$$C_\infty = \frac{\tan\theta_w}{(\sigma/\rho-1)(\tan\phi-\tan\theta_w)} \tag{22}$$

If $0.03 < \tan\theta_w \le 0.138$, an immature type debris

flow occurs, and

$$C_{\infty} = 6.7\left\{\frac{\tan\theta_w}{(\sigma/\rho-1)(\tan\phi-\tan\theta_w)}\right\}^2 \quad (23)$$

If $\tan\theta_w \le 0.03$, a turbulent water flow with bed load transport occurs, and

$$C_{\infty} = \frac{(1+5\tan\theta_w)\tan\theta_w}{\sigma/\rho\ -1}\left(1-\alpha_0^2\frac{\tau_{*c}}{\tau_*}\right)\left(1-\alpha_0^2\sqrt{\frac{\tau_{*c}}{\tau_*}}\right) \quad (24)$$

where ϕ is the internal friction angle of the sediment, and

$$\alpha_0^2 = \frac{2\{0.425-(\sigma/\rho)\tan\theta_w/(\sigma/\rho-1)\}}{1-(\sigma/\rho)\tan\theta_w/(\sigma/\rho-1)} \quad (25)$$

$$\tau_{*c} = 0.04\times10^{1.72\tan\theta_w} \quad (26)$$

$$\tau_* = \frac{h\tan\theta_w}{(\sigma/\rho-1)d_m} \quad (27)$$

in which θ_w is water surface slope, τ_{*c} is the non-dimensional critical shear stress, and τ_* is the non-dimensional shear stress.

4. Results and discussion

Fundamental experiment and numerical simulation are conducted to investigate debris-flow breakers. The parameters of the simulation are as follows;

The effectiveness of deck shape in a debris flow fan was investigated through numerical model and laboratory experiments. To measure the thickness of accurately, a point gauge is used in each point.

To verify the model, the simulated results of outflow discharge and sediment discharge at the downstream end of flume without debris-flow breaker are used. In addition, experimental condition was carried out three times and average values are used.

In fig. 7 is the temporal variations of flow, sediment discharge and sediment concentration in the case of bed sediment-B. Fig. 8 shows the correlation

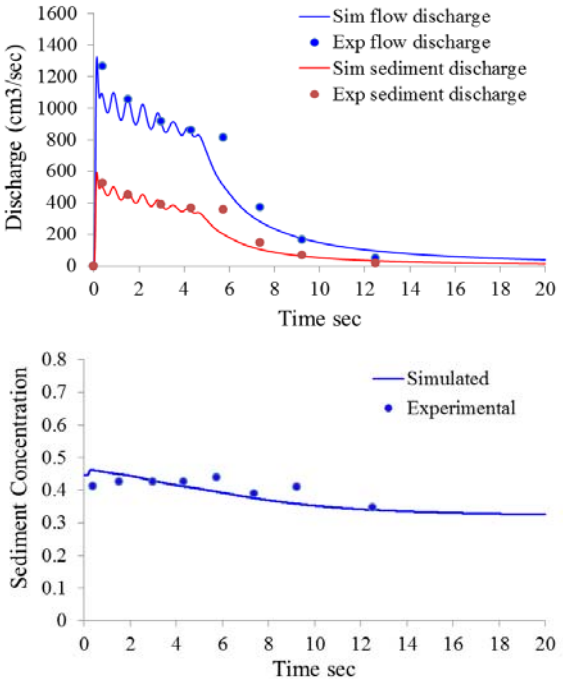

Fig. 7 Numerical and experimental results

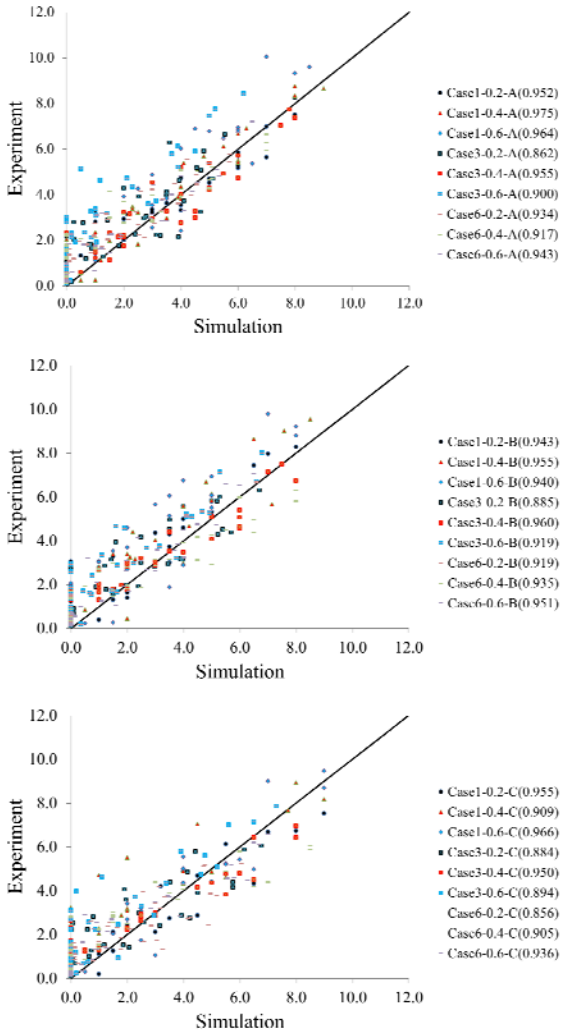

Fig. 8 Correlation coefficient of deposit thickness between simulation and experimental results

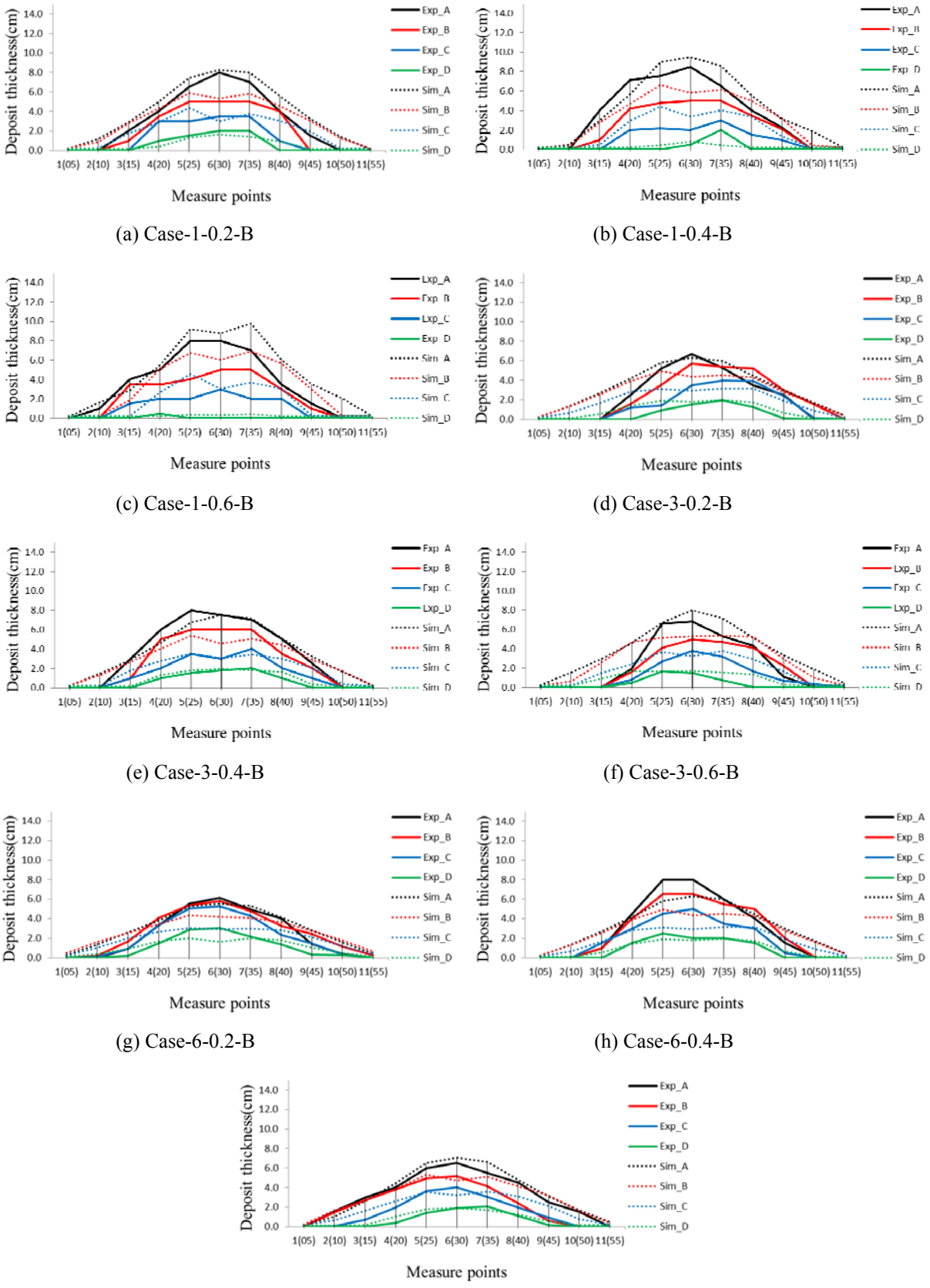

(a) Case-1-0.2-B

(b) Case-1-0.4-B

(c) Case-1-0.6-B

(d) Case-3-0.2-B

(e) Case-3-0.4-B

(f) Case-3-0.6-B

(g) Case-6-0.2-B

(h) Case-6-0.4-B

(i) Case-6-0.6-B

Fig. 9 Comparison of deposition thickness numerical simulation and experimental results

coefficient of deposition thickness for all cases. The observed results of the deposition thickness were almost equal to the numerical ones. But, simulation was slightly larger than experiment. Comparison of deposition thickness and travel length are made using observation points by each case. In fig. 9 from (a) to (i) are the comparison of deposition thickness on the observation points of deck. Simulation results are larger than experiment results. The reasons for this study did not consider separated fine sediment through the opening size.

Table 4 shows that changes in the reduction of travel length depend on blocking size and opening size between experimental, using previous γ coefficient and using new γ coefficient. The results of travel length are good agreement using new γ coefficient more than using previous γ coefficient. The results of experiments have a reduction of range from minimum 30% (Case-6-0.2-B) to maximum 62% (Case-1-0.6-A) by compare Case-0-0-A,B,C with each another case.

Table 4 Results of travel length

No.	Block	Open	Exp	Old γ	New γ
Case-1-0.2-A	1	0.2	42.0	48.5	41.2
Case-1-0.4-A		0.4	40.0	34.3	35.2
Case-1-0.6-A		0.6	30.0	23.0	33.8
Case-3-0.2-A	3	0.2	47.9	52.1	46.3
Case-3-0.4-A		0.4	42.0	50.2	42.0
Case-3-0.6-A		0.6	38.5	48.5	39.3
Case-6-0.2-A	6	0.2	51.1	53.2	48.8
Case-6-0.4-A		0.4	49.0	52.0	46.4
Case-6-0.6-A		0.6	44.1	51.8	44.2
Case-1-0.2-B	1	0.2	39.0	45.6	37.7
Case-1-0.4-B		0.4	34.0	34.2	33.3
Case-1-0.6-B		0.6	30.0	20.5	31.9
Case-3-0.2-B	3	0.2	40.6	49.6	44.6
Case-3-0.4-B		0.4	38.0	48.2	39.9
Case-3-0.6-B		0.6	37.9	45.6	38.9
Case-6-0.2-B	6	0.2	41.0	50.4	45.9
Case-6-0.4-B		0.4	46.0	49.5	44.6
Case-6-0.6-B		0.6	42.8	49.4	41.9
Case-1-0.2-C	1	0.2	35.0	44.3	36.8
Case-1-0.4-C		0.4	26.0	31.6	32.0
Case-1-0.6-C		0.6	28.0	18.2	30.8
Case-3-0.2-C	3	0.2	37.1	48.2	42.0
Case-3-0.4-C		0.4	32.0	46.2	37.5
Case-3-0.6-C		0.6	34.7	44.3	34.6
Case-6-0.2-C	6	0.2	41.1	48.5	43.3
Case-6-0.4-C		0.4	40.0	48.3	42.0
Case-6-0.6-C		0.6	35.2	48.0	39.5

Unit : cm

Fig. 10 shows that attempt an analysis according to experimental results between total opening size(cm), width(cm), max diameter(mm), geometric standard deviation and reduction rate of travel length.

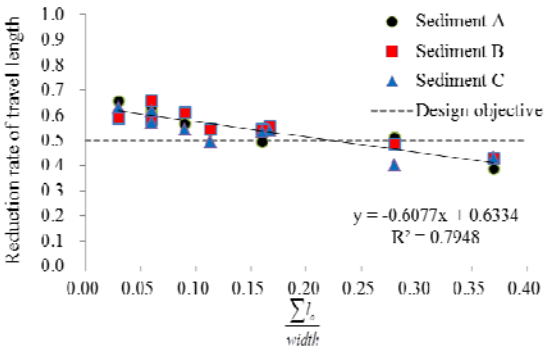

I. Relationship between reduction rate and $\frac{\sum l_o}{width}$

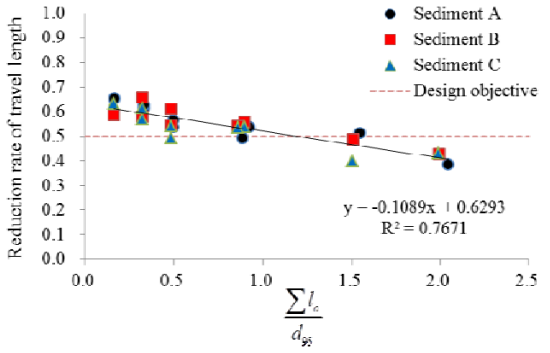

II. Relationship between reduction rate and $\frac{\sum l_o}{d_{95}}$

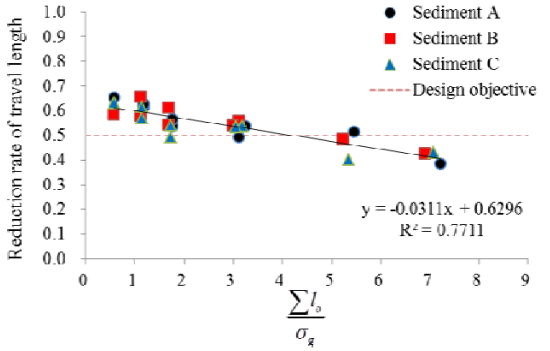

III. Relationship between reduction rate and $\frac{\sum l_o}{\sigma_g}$

Fig. 10 Relationship of suitable range

Geometric standard deviation and reduction rate of travel length are as follow:

$$\sigma_g = 0.5\left(\frac{d_{84}}{d_{50}} + \frac{d_{50}}{d_{16}}\right) \tag{28}$$

$$Reduction \quad rate = \frac{T.L(each \quad cases)}{T.L(without \quad cases)} \tag{29}$$

A great deal of research is being carried out to discover the optimum range of open type sabo dam. Watanabe, et al.(1980) for a given relationship, the volume of the debris flow could be reduced by 50% during peak time. The above studies validated the effectiveness of open-type dams in the prevention of debris flow. They all only considered the relative spacing factor in designing the spacing of open-type dams. Even if debris-flow breaker is also similar to the open- type dam, main of function is some different between silt type and breaker type. In addition, little is known about debris-flow breaker. In this study is aiming to reduction rate of travel length by 50% when evaluating for relationship of range. The relationship(I) have been shown to be effective in reducing rate of 50% reduction rate of travel length as total opening size/width range from 0.19 to 0.24 (sediment A: 0.22, sediment B:0.24, sediment C: 0.19). The relationship(II) have been shown to be effective in reducing rate of 50% reduction rate of travel length as total opening size/max diameter range from 1.1 to 1.3 (sediment A:1.2, sediment B:1.3, sediment C:1.1). The relationship(III) have been shown to be effective in reducing rate of 50% reduction rate of travel length as total opening size/ Geometric standard deviation range from 3.7 to 4.7 (sediment A:4.4, sediment B:4.7, sediment C:3.7).

5. Conclusions

The numerical model is developed to simulate debris flow deposition, and erosion downstream of a debris-flow breaker. A new momentum equation to calculate debris flow deposition downstream of a debris-flow breaker dam is also developed based on the mechanism of changing pressure on the deck due to γ coefficient. The debris flow deposition phenomenon downstream of breaker dam can be calculated by the proposed debris flow model. The simulated results of debris flow deposition downstream of a debris-flow breaker dam, and the erosion of deposited sediment using a two-dimensional riverbed erosion model agree well with the experimental results. From the results, it is shown that the infiltration type sabo dam can reduce their sediment trapping capacity more effectively than the closed bottom infiltration type sabo dam. In addition, we can determine the optimum size using suggested relationship.

Acknowledgements

This research is supported by JSPS AA Science Platform Program (Coordinator: H. Nakagawa).

References

Gonda, Y. (2009): Function of a debris-flow brake, International Journal of Erosion Control Engineering, Vol.2, No.1, pp.15-21.

Huang, X., and Garcia, M.H. (1997): A perturbation solution for Bingham-plastic mudflows, Journal of Hydraulic Engineering, ASCE, Vol.123, No.11, pp.986-994.

Hunt, B. (1994): Newtonian fluid mechanics treatment of debris flows and avalanches, Journal of Hydraulic Engineering, ASCE, Vol.120, No.12, pp.1350-1363.

ICHARM. (2008): Debris-flow dewatering brakes: a promising tool for disaster management in developing countries, International Center for Water Hazard and Risk Management Newsletter, Vol. 3, No. 3, pp.10.

Nakagawa, H., Takahashi, T., Satofuka, Y., and Kawaike, K. (2003): Numerical simulation of sediment disasters caused by heavy rainfall in Camuri Grande basin, Venezuela 1999, Proceedings of the 3rd Conference on Debris-Flow Hazards Mitigation: Mechanics, Prediction, and Assessment, pp.671-682.

Ralph L, Rosnow., Robert, Rosenthal., and Donald B, Rubin. (2000): Contrasts and correlations in effect-size estimation, A Journal of the Association for Psychological Science, Vol. 11, No. 6, pp.446-453.

Suwa, H., Okano, K., and Kanno, T. (2009):

Behavior of debris monitored on test slopes of Kamikamihorizawa Creek, Mount Yakedake, Japan, International Journal of Erosion Control Engineering, Vol. 2, No.2, pp.33-45.
Takahashi, T. (1991): Debris flow, IAHR Monograph Series, Rotterdam: Balkema.
Takahashi, T., Nakagawa, H., Harada, T., and Yamashiki, Y. (1992): Routing debris flows with particle segregation, Journal of Hydraulic.
Takahashi, T., Satofuka, Y., and Chishiro, K. (1997): Dynamics of debris flows in the inertial regime, Proceedings of the 1st Conference on Debris-Flow Hazards Mitigation: Mechanics, Prediction, and Assessment, pp.239-248.
Watanabe, M., Mizuyama, T., and Uehara, S. (1980): Review of debris flow countermeasure facilities, J. of the Japan Erosion Control Engineering Society, Vol. 115, pp.40-48.

(Received 8, June, 2012)

土石流の数値解析と実験的研究

Yeonjoong KIM(1)・中川一・川池健司・Hao ZHANG

(1) 京都大学大学院工学研究科

要　旨

土石流ブレーカーの主な機能は，土石流の先端部を効率的に停止させるものである。また，狭い地域に設置可能，単価が安い，デザインが簡単である，修理が容易という特徴がある。しかし，現在では土石流ブレーカーのメカニズムは，まだ十分に説明されていない。この論文では，土石流ブレーカーに関する基礎的な実験を実施し，そして数値モデルによりその実験の検証計算を実施している。そして，それらの結果から，デッキサイズの変化による圧力変化の方法を提案している。その結果，最適なサイズとデッキ幅，砂の最大直径，幾何標準偏差の関係を明らかにしている。また，数値モデルの計算結果では，デッキ上の移動距離と堆積の高さは実験結果とよく一致する結果が得られた。

キーワード：土石流，間隙水圧，最適サイズ，土石流ブレーカー